**2006 Southern California Earthquake Center Annual Report**
**The Transition from Foreshock to Main shock to Aftershock in California and Japan**

Zhigang Peng (PI)
School of Earth and Atmospheric Sciences
Georgia Institute of Technology, Atlanta, GA, 30338
March 7, 2007

***Summary***

Observations of earthquake triggering, especially the transition from foreshocks to main shock to aftershocks, provide a useful tool to test various models of earthquake interaction, and to constrain the physics of earthquake rupture nucleation, propagation, and arrest. In this project, we mainly focused on the following two directions: (1) late foreshocks and early aftershocks from continuous waveforms in California and Japan; and (2) occurrence patterns of foreshocks in southern California. The various studies are discussed in more detail below.

***Anomalous early aftershock decay rate of the 2004 Mw6.0 Parkfield, California, earthquake***

A large shallow earthquake is typically followed by aftershocks that diminish in rate approximately as the inverse of the elapsed time since the main shock, a phenomenon known as the Omori's law [*Omori*, 1894]. Later, *Utsu et al.* [1995] introduced the modified Omori's law $R(t) = K/(t+c)^p$, where $K$ is the aftershock productivity, $p$ is the exponent that is generally close to 1, and $c$ is a constant time shift. The $c$ value is introduced to eliminate the singularity in the aftershock rate as $t$ goes to zero.

Since it is difficult to observe early aftershock activity in the noisy aftermath of large earthquakes, the existence of the $c$ value and its physical meaning are still under debate [e.g., *Utsu et al.*, 1995; *Kagan*, 2004; *Peng et al.*, 2006, 2007]. Yet this period marks the transition from main shock to aftershocks, and holds valuable information about the underlying mechanisms that control the aftershock occurrence [e.g., *Das and Scholz*, 1981; *Dieterich*, 1994; *Ben-Zion and Lyakhovsky*, 2006].

We systematically analyzed the early aftershock decay rate of the 2004 Mw6.0 Parkfield, California, earthquake [*Bakun et al.*, 2005] by scrutinizing high-frequency signals from seismograms recorded near the source region. Since seismic codas of the main shock have little high frequency content, we apply a two-pass Butterworth high-pass filter to detect early aftershocks buried inside the main shock coda. A total of 46 events within 300 s after the main shock are identified from the high-pass-filtered envelope at station PKD (Figure 2). In comparison, only two aftershocks (and the main shock itself) are listed in the NCSN catalog in this time period. A total of 72 events are listed in the NCSN catalog within the first hour after the main shock. In comparison, we identified 247 events during the same period. This indicates that the commonly observed $c$ values (on the order of a few hours or more) are most likely caused by missing aftershocks in the catalog.

Next, we estimate the seismicity rate immediately after the Parkfield main shock by summing the envelope values well above the noise in each time window (Figure 3). Although the rate computed from the envelope fluctuates more than that from the catalog, the seismicity rates estimated from different methods are similar. We note that the seismicity rate in the first few hundred seconds is approximately steady, instead of following the same decay rate as at later times (Figure 3). We use Bayesian Information Criterion (BIC) to quantify the statistical significance of such a break of slope in the seismicity rate [*Main et al.*, 1999]. The peak of the

BIC values for the double-slope model is higher than that for the single-slope model (Figure 4), indicating that the break of slope in the seismicity rate is statistically significant. The break point $t^*$ = 132 s is found when the BIC reaches its maximum value. The best fitting $p$ values are –0.18±0.20 between 30 and 132 s, and 0.74±0.03 between 132 and $10^6$ s.

Our results suggest a distinct early stage of low aftershock activity that marks a transition from main shock rupture to numerous aftershocks, which we refer to as Early Aftershock Deficiency (EAD). This result argues against a model in which main shock rupture propagation is represented as no more than the superposition of aftershocks [*Kagan*, 2004], and suggests that a main shock rupture and its aftershock sequence are distinct processes, not described by a single Omori's law. Our observation of a near-constant seismicity rate immediately after the main shock is consistent with the predictions of several physical models for aftershock processes, including the rate- and state-dependent friction model [e.g., *Dieterich*, 1994], the stress corrosion model [e.g., *Gomberg*, 2001], and the damage rheology model [*Ben-Zion and Lyakhovsky*, 2006]. Additional information, such as long-term seismicity rate, thermal gradient, loading rate, and seismic coupling, is needed to distinguish among these models.

***Foreshock occurrence pattern in southern California***

In the second work [*Peng*, 2007], we study the occurrence patterns of foreshocks in southern California using the relocated catalog of *Shearer et al.* [2005]. We search for earthquake sequences that are well separated in space and time with other events. A main shock in each sequence is defined as any earthquake that is not preceded and followed by larger events within 50 km and 100 days of that event. Immediate foreshocks and aftershocks are those within 5 km and 5 days before and after the main shock, respectively. After the selection, process, we identify 106 sequences that spans most of our study region (Figure 5).

Following the definition of *Mogi* [1963], we classify the 106 sequences into three types: A) sequences without immediate foreshocks; B) sequences with immediate foreshocks; C) earthquake swarms. To separate type B and C, we use the following empirical rules: 1) the sum of immediate foreshocks and aftershocks is at least 10; 2) the number of foreshocks is larger than the number of aftershocks, or the magnitude of the largest foreshocks/aftershocks is less than 0.5 magnitude unit of the main shock. The first rule ensures that the seismicity rate of the swarms is significantly higher than the background rate. The second rule ensures that the main shock is not the driving force for that sequence.

As shown in Figure 5, there is a clear geographic pattern for different type of sequences. Most type A sequences (no immediate foreshocks) are located in the Los Angeles Basin, Transverse Ranges, and off the coast of California. Some sequences near the Garlock fault and east of the Sierra Nevada Mountain belong to type A. The majority of sequences around the south-eastern end of Sierra Nevada mountains, the Eastern California Shear Zone, and the Salton Sea area belong to type B (with immediate foreshocks). Earthquake swarms (type C) have similar locations as type B sequences. The geographic pattern is similar to previous studies using M>=5 mainshocks in the same region [*Abercrombie and Mori*, 1996]. This indicates that the foreshock occurrence patterns do not change with main shock magnitude. The major difference between our and previous studies is that we include more intermediate-size main shocks for better statistics.

We note that the geographic patterns on different types of sequences positively correlates with the surface heat flow (http://earthquake.usgs.gov/heatflow/index.html), and the main shock depth (Figure 6a). In addition, there is a weak correlation between foreshock occurrence and main shock slip orientation (Figure 6b). We speculate that structural properties, such as small-scale crustal heterogeneities, and partition between seismic and aseismic deformation in each region

play a dominant role in controlling foreshock generation. In addition, increase of normal stress may inhibit the occurrence of foreshocks [e.g., *Abercrombie and Mori*, 1996]. Further analysis is needed to differentiate different mechanisms that control the spatial patterns of foreshock occurrence.

**References**


Abercrombie, R. E. and J. Mori (1996), Occurrence patterns of foreshocks to large earthquakes in the western United States, *Nature*, 381, 303-307.

Bakun, W. H. *et al.* (2005), Implications for prediction and hazard assessment from the 2004 Parkfield earthquake, *Nature*, *437*, 969–974, doi: 10.1038/nature04067.

Ben-Zion, Y. and V. Lyakhovsky (2006), Analysis of Aftershocks in a Lithospheric Model with Seismogenic Zone Governed by Damage Rheology, *Geophys. J. Int.*, *165*, 197-210.

Das, S., and C. Scholz (1981), Off-fault aftershock clusters caused by shear stress increase?, *Bull. Seismol. Soc. Am.*, *71*, 1669–1675.

Dieterich, J. H. (1994), A constitutive law for rate of earthquake production and its application to earthquake clustering, *J. Geophys. Res.*, *99*, 2601–2618.

Gomberg, J. (2001), The failure of earthquake failure models, *J. Geophys. Res.*, *106*(B8), 16,253–16,264.

Kagan, Y. Y. (2004), Short-term properties of earthquake catalogs and models of earthquake source, *Bull. Seismol. Soc. Am.*, *94*(4), 1207–1228.

Main, I. G., T. Leonard, O. Papasouliotis, C. G. Hatton, and P. G. Meredith (1999), One slope or two? Detecting statistically-significant breaks of slope in geophysical data, with application to fracture scaling relationships, *Geophys. Res. Lett.*, *26*, 2801–2804.

Mogi, K. (1963), Some discussions on aftershocks, foreshocks, and earthquake swarms: The fracture of a semi-infinite body caused by an inner stress origin and its relation to the earthquake phenomenon, *Bull. Earthquake Res. Inst. Univ. Tokyo*, 41, 615–658.

Omori, F. (1894), On the aftershocks of earthquakes, *J. Coll. Sci. Imp. Univ. Tokyo*, *7*, 111–200.

* Peng, Z. (2007), Occurrence patterns of foreshocks and aftershocks in southern California, submitted to the Seismological Society of America Annual Meeting, Big Island, Hawaii.

* Peng, Z., J. E. Vidale, and H. Houston (2006), Anomalous early aftershock decay rates of the 2004 M6 Parkfield earthquake, *Geophys. Res. Lett.*, 33, L17307, doi:10.1029/2006GL026744.

* Peng, Z., J. E. Vidale, M. Ishii, and A. Helmstetter (2007), Anomalous seismicity rates immediately before and after main shock rupture from high-frequency waveforms in Japan, *J. Geophys. Res.*, in press.

Shearer, P.M., E. Hauksson, and G. Lin (2005), Southern California hypocenter relocation with waveform cross-correlation: Part 2. Results using source-specific station terms and cluster analysis, *Bull. Seism. Soc. Am.*, 95, 904–915.

Utsu, T., Y. Ogata, and R. S. Matsu'ura (1995), The centenary of the Omori formula for a decay law of aftershock activity, *J. Phys. Earth*, *43*(1), 1–33.


* Publications supported by this proposal.

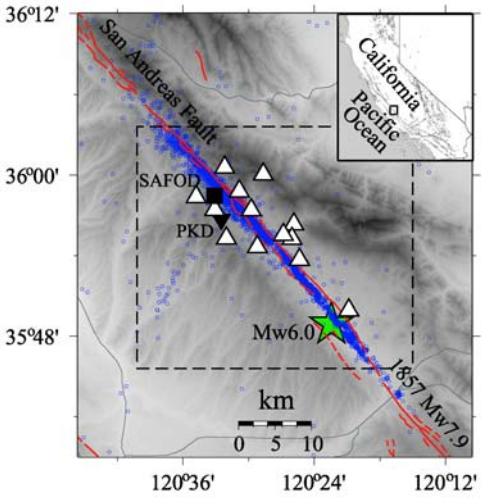


Figure 1. Map of the study area, including the epicentral location of the 2004 Mw6.0 Parkfield earthquake (green open star), and aftershocks listed in the Northern California Seismic Network (NCSN) catalog (blue dots). The red and gray lines denote the surface traces of the San Andreas fault, and the nearby highways, respectively.

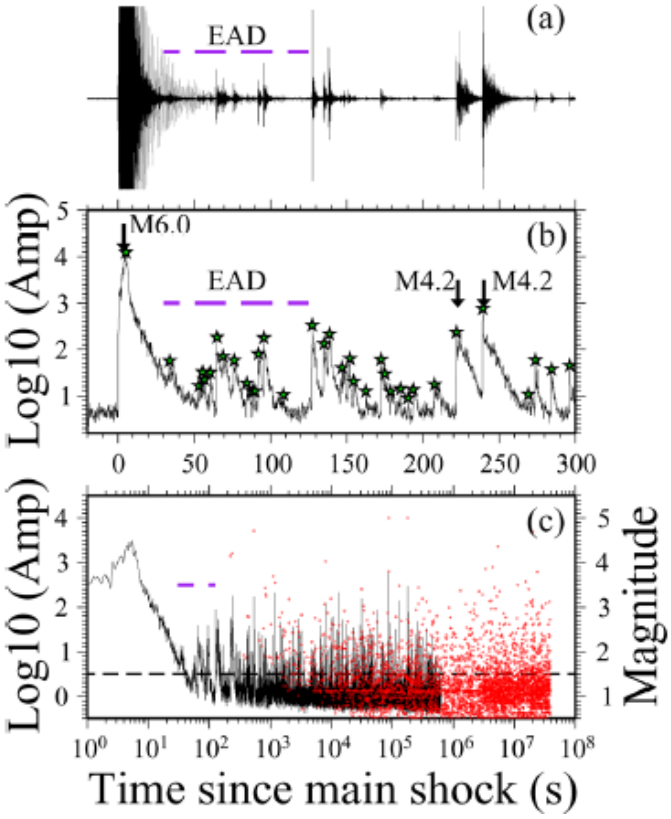


Figure 2. (a) Original (gray line) and high-pass-filtered (dark line) vertical-component seismogram recorded by station PKD. The trace is clipped, with the peak amplitude of the main shock off-scale. (b) Logarithm of the envelope (dark line) generated by stacking the envelopes of the high-pass-filtered three component seismograms for station PKD. Each blue star marks an event identified by our handpicking procedure. (c) Comparison between the envelope for station PKD (gray line) and aftershocks (small red dots) listed in the NCSN catalog in logarithmic time scale. The envelope level has been shifted so that the pre-event noise level is zero. The horizontal dashed line marked the cutoff amplitude of 0.5 (in logarithmic scale) above which the amplitudes are summed to obtain the seismicity rate in Figure 3.

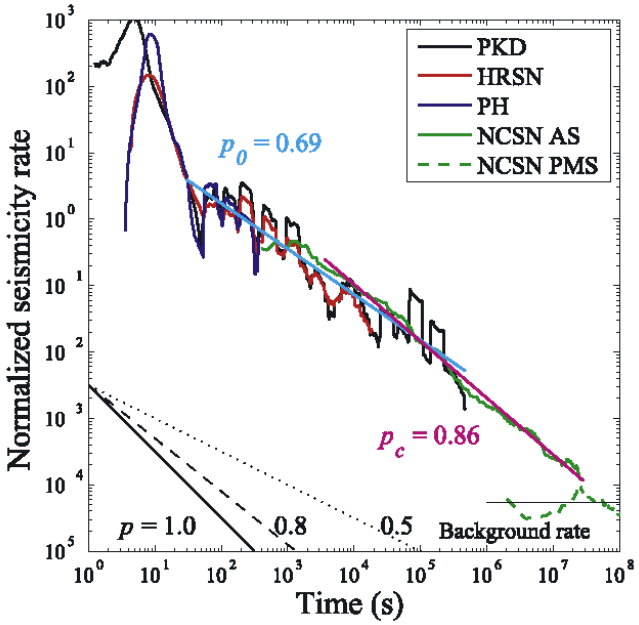


Figure 3. Aftershock seismicity rates as a function of the time since the main shock obtained from the high-pass-filtered envelopes for station PKD (dark line), HRSN array (red line), SAFOD Pilot Hole array (blue line), and from the NCSN catalog with $m \geq 1.5$ (green line). The cyan and magenta lines denote least-squares fitting for the seismicity rate observed at station PKD in the time interval of [30 – $6.3 \times 10^5$] s, and from the NCSN aftershocks in the time interval of [3600 – $2.9 \times 10^7$] s. The obtained $p$ values are listed. The solid, dashed and dotted lines show the reference rates with $p$ = 1.0, 0.8, and 0.5.

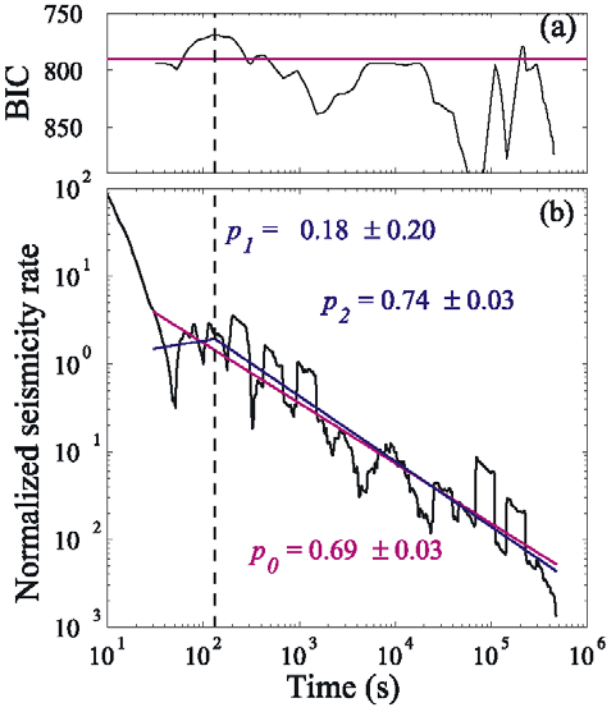


Figure 4. (a) The Bayesian Information Criterion (BIC) plotted as a function of the change point $t^*$ for a double-slope model (the dark line), compared with a single-slope model (the magenta line) for seismicity rate at station PKD. The dashed vertical line marks the location of the best fitting break of slope. (b) Seismicity rate as a function of the time since the main shock obtained from the high-pass-filtered envelopes for station PKD. The best fitting lines using the single-slope model (the magenta line) and the double-slope model (the blue line) are shown. The obtained $p$ values are listed.

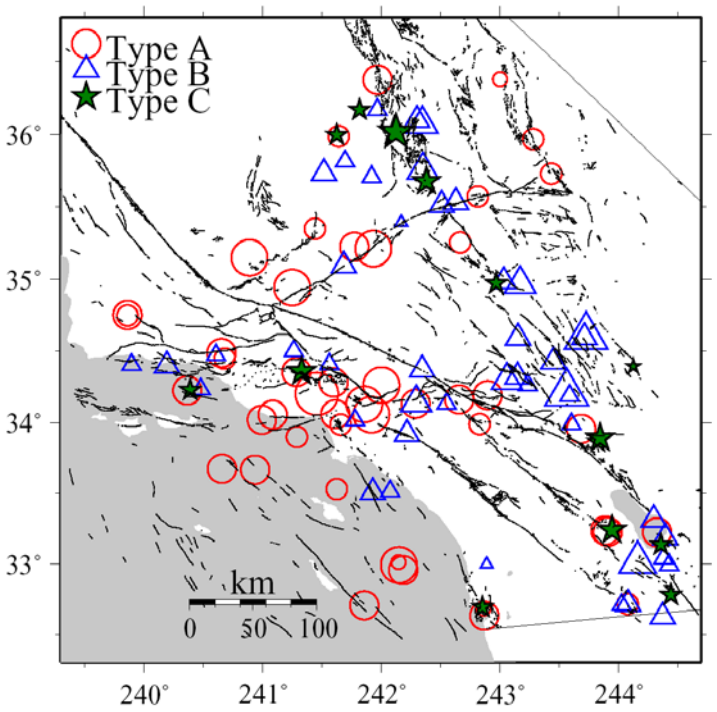


Figure 5. Occurrence patterns for different types of earthquake sequences in southern California. Red circles indicate 46 earthquakes with no immediate foreshocks (type A). Blue triangles mark 45 earthquakes preceded by immediate foreshocks (type B). Filled blue stars denote 15 sequences that are categorized as swarms (type C). The dark lines denote the surface traces of active faults.

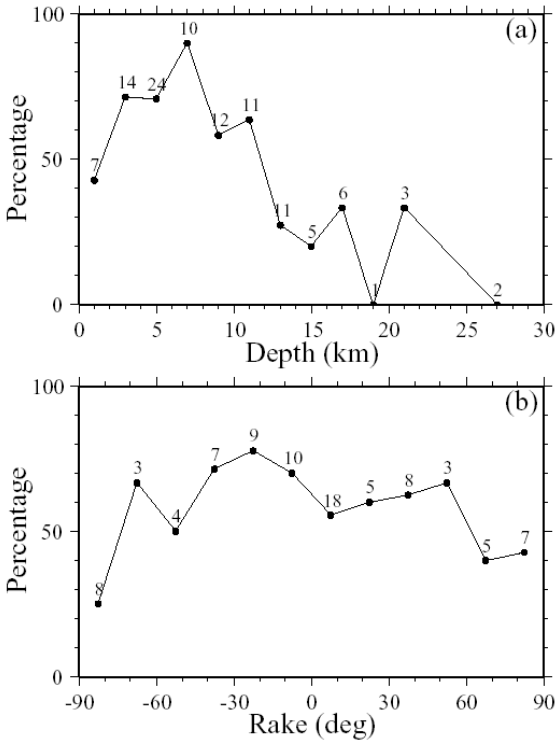


Figure 6. The percentage of foreshock occurrence as a function of main shock (a) depth and (b) rake. The number above each data point corresponds to the total number of main shocks in that interval. A rake of –90°, 0°, and 90° corresponds to pure normal, strike-slip, and thrust faulting events, respectively.